



HAL
open science

Friction Experiments for Filament Winding Applications

Sotiris Koussios, Otto K. Bergsma

► **To cite this version:**

Sotiris Koussios, Otto K. Bergsma. Friction Experiments for Filament Winding Applications. *Journal of Thermoplastic Composite Materials*, 2006, 19 (1), pp.5-34. 10.1177/0892705706049561 . hal-00570797

HAL Id: hal-00570797

<https://hal.science/hal-00570797>

Submitted on 1 Mar 2011

HAL is a multi-disciplinary open access archive for the deposit and dissemination of scientific research documents, whether they are published or not. The documents may come from teaching and research institutions in France or abroad, or from public or private research centers.

L'archive ouverte pluridisciplinaire **HAL**, est destinée au dépôt et à la diffusion de documents scientifiques de niveau recherche, publiés ou non, émanant des établissements d'enseignement et de recherche français ou étrangers, des laboratoires publics ou privés.

Friction Experiments for Filament Winding Applications

SOTIRIS KOUSSIOS* AND OTTO K. BERGSMA

*Department of Design and Production of Composite Structures
Faculty of Aerospace Engineering
Delft University of Technology
Kluyverweg 1, 2629 HS Delft
The Netherlands*

ABSTRACT: The design procedure of nongeodesic filament wound products requires well-determined values for the available friction situated between the applied roving and the supporting surface. In this paper, we propose a mandrel shape with a specially designed meridian profile that enables a linearly proportional relation between the feed eye carriage translation and the measured values for the coefficients of friction. As a result of this property, the optically or chronometrically obtained measurements can directly be translated into coefficients of friction. Additional features of this approach are the high accuracy, repeatability, low experimental costs, and simple machine control strategies. With the proposed mandrel, we performed several experiments corresponding to the variation of typical filament winding-related process parameters: fiber speed, roving tension, roving dimensions, wet versus dry winding, and surface quality of the mandrel. The results indicate that the surface quality of the mandrel and the type of winding process (wet vs. dry fibers) have a considerable influence on the obtained data. The influence of the fiber speed, roving tension, and fiber material on the other hand, is negligible.

KEY WORDS: filament winding, nongeodesics, friction measurements.

INTRODUCTION

THE STEADILY INCREASING field of filament winding applications involves, nowadays, an extensive variety of products [1,2]. The reinforcement layer architecture is mostly based on geodesic towpaths. For the majority of applications, geodesic towpaths provide minimum length trajectories, thus lower weight. For several composite structures however,

*Author to whom correspondence should be addressed. E-mail: KoussiosS@dutlbez.lr.tudelft.nl

the implementation of nongeodesic fiber trajectories certainly increases the design space [3–5]. A typical example of this design space expansion is the geometric determination of nongeodesic isotensoidal pressure vessels; the ability for modifying the winding angle (around the values provided by geodesic paths) introduces an additional degree of freedom for the mandrel shape determination [3]. An additional application is the creation of transitional circuits for cylindrical pressure vessels enabling a smooth change from polar circuits to hoop ones [5]. The most promising application however, is the generation of rotational symmetric objects (e.g., beams and struts) providing the optimal winding angle distribution for particular load situations.

The creation of nongeodesic towpaths requires a well-determined value for the available friction between placed roving and supporting surface (mandrel) [6–10]. For the determination of the corresponding coefficient of friction through experimental ways, several methods have been developed [3,11,13]. The most realistic method is the measurement of friction on a rotationally symmetric mandrel, attached on a filament-winding machine. The mandrel shape is usually generated with an elliptical meridian profile [3]. This profile can be characterized by a wide range of normal and geodesic curvatures. Consequently, an extensive range for the coefficients of friction can be measured. The measured values however, are generally not in linear relationship with at least one of the filament-winding machine movements. This property usually introduces particular difficulties related to the implementation of the obtained measurements.

To overcome the problems of measurement stability and linearity, we introduce here a meridian profile providing a linear relationship between the feed eye carriage translation along the axis of the mandrel rotation and the measured coefficients of friction. This linearity enables a fast and facilitated interpretation of the measurements obtained by for example, optical methods (high shutter speed camera). The carriage coordinate where roving slipping occurs can directly be translated into a coefficient of friction. In addition, the machine control becomes rather simple; the corresponding CNC data for the controller can easily be created with a spreadsheet program. With the specially designed mandrel attached on a lathe-configured winding machine, we performed several experiments corresponding with parameter combinations that are typical for filament winding applications: winding speed, roving tension, roving morphology, wet versus dry fibers, and surface quality of the mandrel.

After the treatment of nongeodesic towpaths on generic shells of revolution in the next section, we present a brief overview of the available friction-measuring methods. A major part of this paper (“Determination of Coefficient of Friction: Mandrel Design”) is associated with the determination of the mandrel shape, providing the previously indicated

linearity between feed eye carriage translation and measured coefficient of friction. This section concludes with an error analysis for inaccuracies, mainly induced by using the simplified solution for the required meridian profile. The section on “Machine Control” provides several tools for the determination of the winding machine movements and the control of the fiber speed. The section on experiment presents a brief description of the experiments (series and error analysis) conducted in this study. The experimental results are presented and discussed in the next section. The paper ends with the formulation of several conclusions regarding the applicability and advantages provided by the proposed mandrel geometry, and a short discussion of the obtained experimental results. In addition, we provide here some recommendations.

NONGEODESIC FIBER TRAJECTORIES ON GENERIC SHELLS OF REVOLUTION

In this section, we outline the basic theory supporting the creation of nongeodesic trajectories on generic shells of revolution. With a general formulation in curvatures and coefficients of the first fundamental form, the basic path equations are derived. These equations show in a clear way the relation between the required friction and curvatures at a point belonging to a convex surface.

We consider here an elementary piece of a convex surface generated by a shell of revolution. The fiber path, attached on the presented surface element, is generally characterized by two radii of curvature (Figure 1): the normal one R_n (vertical to the surface element), and the so-called geodesic curvature, (located in-plane of that surface).

The fiber is subjected to a longitudinal force F , a normal force per unit length f_n and a lateral force per unit length f_μ . The static equilibrium of the forces vertical and lateral to the surface can be expressed as follows:

$$f_n R_n \Delta\varphi = 2F \sin\left(\frac{\Delta\varphi}{2}\right) \approx F \Delta\varphi \Rightarrow f_n = \frac{F}{R_n} \quad (1)$$

$$f_\mu R_g \Delta\omega = 2F \sin\left(\frac{\Delta\omega}{2}\right) \approx F \Delta\omega \Rightarrow f_\mu = \frac{F}{R_g} \quad (2)$$

The lateral fiber force is ensured by friction occurring between the fiber bundle and the surface. The condition for fiber placement stability is [3–15]:

$$\mu \geq \left| \frac{f_\mu}{f_n} \right| = \left| \frac{F/R_g}{F/R_n} \right| = \left| \frac{R_n}{R_g} \right| = \left| \frac{k_g}{k_n} \right| \quad (3)$$

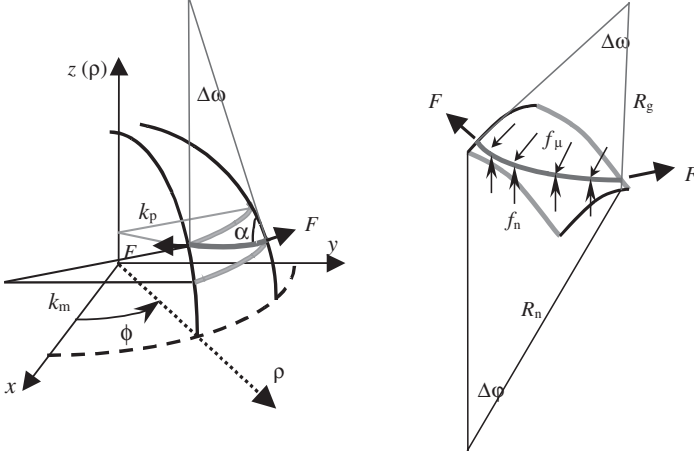


Figure 1. Elementary piece of a fiber on a shell of revolution: curvatures and acting forces.

where k_n and k_g represent the normal and geodesic curvature (dimension: 1/length) respectively, and μ stands for the maximum available value for the coefficient of friction. In the case of applying geodesic trajectories, the geodesic curvature becomes zero; this immediately leads to the conclusion that geodesic fiber paths do not require any friction between mandrel and roving.

The required friction for towpath stability can be determined by the ratio of the normal and geodesic curvature (Equation (3)). We provide here the theoretical background for the calculation of these quantities. The parametric description of the shell of revolution depicted in Figure 1, is:

$$\mathbf{S} : U \rightarrow \mathfrak{R}^3 : \mathbf{S}(\rho, \phi) = \{\rho \cos \phi, \rho \sin \phi, z(\rho)\} \quad (4)$$

The coefficients of the first and second fundamental forms are closely related with the metrics and principal curvatures of a surface [16–18]:

$$\begin{aligned} E = |\mathbf{S}_\phi|^2 = \mathbf{S}_\phi \cdot \mathbf{S}_\phi = E(\phi) = \rho^2 & & e = \frac{\det[\mathbf{S}_{\phi\phi}, \mathbf{S}_\rho, \mathbf{S}_\phi]}{\sqrt{EG - F^2}} = \frac{-|\rho|z'(\rho)}{\sqrt{1 + z'^2(\rho)}} \\ F = \mathbf{S}_\phi \cdot \mathbf{S}_\rho = 0 & & f = \frac{\det[\mathbf{S}_{\rho\phi}, \mathbf{S}_\rho, \mathbf{S}_\phi]}{\sqrt{EG - F^2}} = 0 \\ G = |\mathbf{S}_\rho|^2 = \mathbf{S}_\rho \cdot \mathbf{S}_\rho = G(\rho) = 1 + z'^2(\rho) & & g = \frac{\det[\mathbf{S}_{\rho\rho}, \mathbf{S}_\rho, \mathbf{S}_\phi]}{\sqrt{EG - F^2}} = \frac{-\text{sgn}(\rho)(z(\rho))}{\sqrt{1 + z'^2(\rho)}} \end{aligned} \quad (5)$$

It should be noted that the parameter E corresponds with the radial metric (parallel direction), while G is directly related to the curve length differential along the meridian ($\phi = \text{constant}$). The principal curvatures of a surface are given by [16,18]:

$$k_{1,2} = \frac{(Eg + eG) - 2Ff \pm \sqrt{(Eg - eG)^2 + 4(Ef - eF)(Gf - gF)}}{2(EG - F^2)} \quad (6)$$

For a shell of revolution, the coefficients F and f are equal to zero (Equation (5)). From Equations (5) and (6) we obtain:

$$\begin{aligned} k_1(\rho) &= \frac{g}{G} = k_m(\rho) = -\frac{z(\rho)}{(1 + z'^2(\rho))^{3/2}} \\ k_2(\rho) &= \frac{e}{E} = k_p(\rho) = -\frac{z'(\rho)}{\rho\sqrt{1 + z'^2(\rho)}} \end{aligned} \quad (7)$$

where the subscripts m and p denote the meridian and parallel direction, respectively. The fiber path orientation is expressed by the parameter α ; this scalar quantity denotes the angle between the path itself and the crossing meridian at the point under consideration. According to Euler, the normal curvature can be expressed as follows [4,11,16,18]:

$$k_n(\rho) = k_m(\rho) \cos^2 \alpha(\rho) + k_p(\rho) \sin^2 \alpha(\rho) \quad (8)$$

Substitution of Equation (7) into (8) leads to:

$$k_n(\rho) = -\frac{\sin^2 \alpha(\rho)[z'(\rho)(1 + z'^2(\rho))/\rho] + \cos^2 \alpha(\rho)[z''(\rho)]}{(1 + z'^2(\rho))^{3/2}} \quad (9)$$

For the shell under consideration, the geodesic curvature is given by [4,11,16]:

$$k_g(\rho) = -\alpha'(\rho) \frac{\cos \alpha(\rho)}{\sqrt{G(\rho)}} - \frac{1}{2} \frac{E'(\rho)}{E(\rho)} \frac{\sin \alpha(\rho)}{\sqrt{G(\rho)}} = -\frac{\alpha'(\rho)\rho \cos \alpha(\rho) + \sin \alpha(\rho)}{\rho\sqrt{1 + z'^2(\rho)}} \quad (10)$$

DETERMINATION OF COEFFICIENT OF FRICTION: MANDREL DESIGN

The basic idea supporting the development of the experiments presented here is that the measurements for the friction coefficient should be as realistic as possible. This is mainly achieved by performing these

experiments on a filament-winding machine, using a rotationally symmetric mandrel. The stability of the obtained measurements should be provided by a linear relation between the coefficients of friction and the translation of the feed eye carriage of the winding machine. After a short overview of the available experimental methods, the final choice is motivated and followed by the geometrical description of the resulting mandrel shape. The section concludes with an error analysis regarding the reliability of the results to be obtained.

Overview and Selection of Experimental Setup

A short overview of the available experimental methods is presented in Table 1 [11,13].

The demands on the experiments to be performed are:

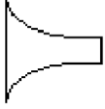
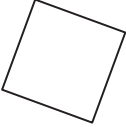
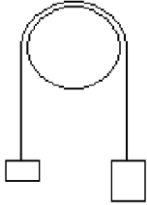
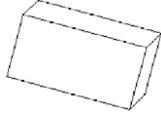
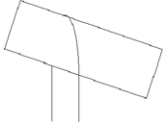
- Realistic simulation of slippage during filament winding
- Inclusion of the consumed fiber speed as an experimental parameter
- Ability for investigating the influence of the fiber tension
- Simple and reliable acquisition of the experimental results

Despite the simplicity of various methods presented in Table 1, the decision is taken in favor of the specially shaped convex mandrel, attached on a lathe-configured filament-winding machine; this combination is the only one satisfying the complete set of requirements. A schematic overview of the chosen configuration is presented in Figure 2.

The movements required for the performance of the experiments are the spindle rotation C , the carriage translation Z , and the feed eye roller inclination A [19]. The latter ensures a tangential placement of the fiber bundle on the mandrel. However, since this movement is not of primary importance for the underlying kinematic model, it is not presented in Figure 2.

The slippage can be determined by optical methods, for example a high shutter speed video camera. When the mandrel is equipped with a benchmark indicating the Z -coordinate, the corresponding coefficient of friction at the moment of fiber slippage can accurately be determined. The increments on the Z -benchmark can be subdivided by placing an additional C -benchmark on the biggest periphery of the mandrel (Figures 9 and 10). An alternative method is to measure the time the roving needs to reach its slippage point when departing from the cylindrical part (in the figure: left side). This method however, might not be very accurate. Nevertheless, since no video camera is needed, it is more economical.

Table 1. Overview of experimental methods for the determination of the coefficient of friction.

Auxiliary apparatus	Winding machine		Tilting apparatus		Arbitrary fixation of gliding plane
Gliding plane	Specially shaped mandrel 	Cylindrical mandrel 	Trumpet-shaped mandrel 	Arbitrary mandrel 	Flat plane 
Procedure	Winding with $\alpha \approx \text{constant}$ till fiber slips	Winding with $\alpha \neq \text{constant}$ till fiber slips	Two different forces, increase one till fiber slips 	Block with roving on the underside will slip at a certain inclination angle 	One roving will slip at a certain inclination angle 
Slip determination	Via fiber tension, optically or time	Via fiber tension or optically	Optically	Optically	Optically

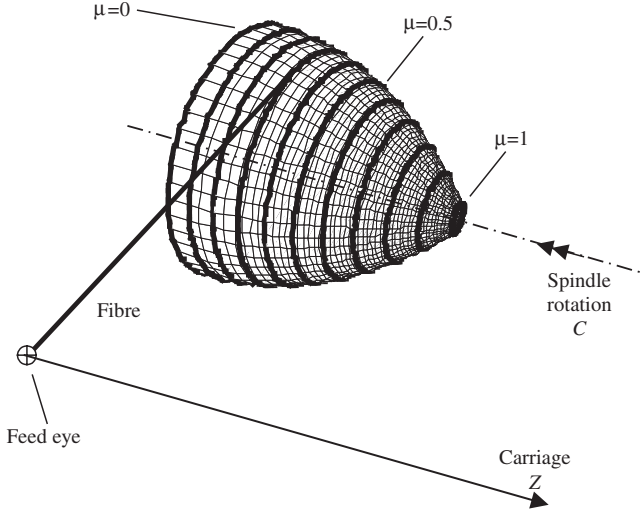


Figure 2. Schematic view of the experimental layout (the bold lines on the mandrel represent a coefficient of friction increment equal to 0.1).

Mandrel Shape

Although any convex meridian profile can generate a proper mandrel shape for the friction experiments, we introduce here an additional requirement; the increase of friction along the meridian profile must be linearly proportional to the translation of the carriage Z by a constant winding angle. The advantages provided by this demand are:

- Facilitated determination of the coefficient of friction by measurement of Z
- Stability of the measurements
- Simple machine control

The fiber bundle is placed on the mandrel at a constant winding angle (in the figure: the fiber orientation is perpendicular to the axis of rotational symmetry of the mandrel). This implies that the carriage is directly coupled to the shape coordinate $z(\rho)$. The linearity requirement for the coefficient of friction μ can now be formulated:

$$\mu(\rho) = c_0 + c_1 z(\rho) \quad (11)$$

The expected coefficients belong to the range $\mu = [0, 1]$ corresponding with $z = [0, z_r]$. These intervals result in:

$$c_0 = 0 \quad c_1 = \frac{1}{z_r} \quad (12)$$

For reasons to be explained later, we assume here: $z_r = 235$ (mm). Depending on the width of the tested fiber bundle, the winding angle becomes:

$$\alpha(\rho) = \frac{\pi}{2} - \varepsilon, \quad 0 \leq \varepsilon \leq 0.1 \text{ (rad)} \quad (13)$$

For a convex meridian profile, the first and second derivatives (respectively $z'(\rho)$ and $z''(\rho)$) are negative. As a result of this, the curvature quotient $k_g(\rho)/k_n(\rho)$ will become negative (Equations (9) and (10)). In addition, the basic static equilibrium equation does not provide any information regarding the sign of the coefficient of friction. In order to generate positive friction values (as dictated by Equation (11)) we multiply the curvature coefficient (k_g/k_n) by -1 . Substitution of Equation (13) into Equations (9) and (10) results in:

$$\mu(\rho) = -\frac{k_g(\rho)}{k_n(\rho)} = -\frac{\cos \varepsilon [1 + z'(\rho)^2]}{\cos^2 \varepsilon [z'(\rho) + z'^3(\rho)] + \rho \sin^2 \varepsilon z'(\rho)} \quad (14)$$

Since ε represents a small angular value, it is justified to neglect the last term in the denominator of Equation (14). The simplified ODE for the meridian profile can then be formulated by the combination of Expressions (11) and (14):

$$\mu_s(\rho) = -\frac{\cos \varepsilon [1 + z'(\rho)^2]}{\cos^2 \varepsilon [z'(\rho) + z'^3(\rho)]} = -\frac{1}{z'(\rho) \cos \varepsilon} = c_0 + c_1 z(\rho) \quad \text{with } z(r) = z_r \quad (15)$$

where r is the minimum mandrel radius (c_0 and c_1 are presented in Equation (12)). The solution of Equation (15) becomes:

$$z_s(\rho) = \sqrt{z_r [z_r + 2(r - \rho) \sec \varepsilon]} \quad (16)$$

The measured coefficient of friction is then given by (Equations (11) and (12)):

$$\mu_m(\rho) = \frac{\sqrt{z_r [z_r + 2(r - \rho) \sec \varepsilon]}}{z_r} \quad (17)$$

For the mandrel design, we assume here that ε is equal to zero. Except the convex part, the mandrel includes an axle for attachment at the winding

machine, and a cylindrical part to provide sufficient space to the fiber bundle for obtaining its targeted velocity during the performance of the experiments. The minimum radius is equal to 15 (mm). At $z_s(\rho)=0$, the maximum radius becomes equal to $r + z_r/2 = 132.5$ (mm).

The experiments are designed to be performed by one person. According to the Dutch labor regulations, the total weight of the mandrel should not exceed the value of 25 (kg) [13]. With $z_r = 235$ (mm) and an aluminum alloy as construction material, the total weight becomes equal to 24.9 (kg). The shape of the resulting mandrel is depicted in Figure 3.

The cylindrical part has a length of 30 (mm); the total length of the axle is 550 (mm). The surface of the mandrel is polished. For a three-dimensional impression of the convex mandrel part, we refer to Figures 2, 9, and 10 (notice in Figure 2 the rings at several z -values indicating the coefficient of friction with incremental steps of 0.1, starting at $\mu = 0$ and ending at $\mu = 1$).

Error Analysis

In the previous subsection, we presented the simplified solution for the mandrel geometry. We assumed a constant winding angle $\alpha = \pi/2 - \varepsilon$, where $\varepsilon \in [0, 0.1]$ (rad). The final shape is designed with $\varepsilon = 0$ (rad). In reality however, the winding angle is equal to:

$$\alpha(\rho) = \text{ArcTan}\left(\frac{2\pi\rho}{b}\right) \quad (18)$$

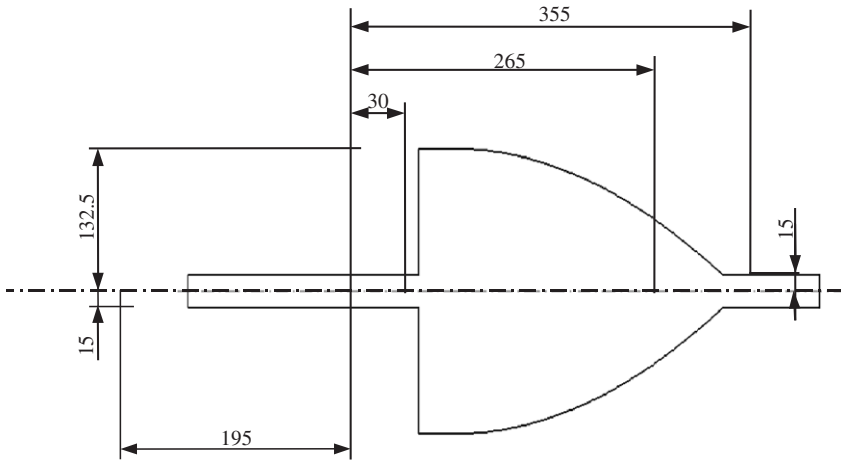


Figure 3. Dimensions of the resulting mandrel shape in (mm).

where b is the width of the tested fiber bundle. Substitution of Equation (18) into Equations (9) and (10) results in:

$$\mu(\rho) = -\frac{k_g(\rho)}{k_n(\rho)} = -\frac{4\pi[b^2 + 2\pi^2\rho^2][1 + z^2(\rho)]}{\sqrt{1 + (4\pi^2\rho^2/b^2)}\{4\pi^2b\rho[z'(\rho) + z^3(\rho)] + b^3z''(\rho)\}} \quad (19)$$

To obtain the real friction values $\mu_r(\rho)$, we substitute Equation (16) into (19). The result is:

$$\begin{aligned} \mu_r(\rho) &= \left(\frac{2\pi(b^2 + 2\pi^2\rho^2) \cos \varepsilon [4(\rho - r) \cos \varepsilon - z_r(3 + \cos 2\varepsilon)]}{\sqrt{b^2 + 4\pi^2\rho^2} \{ [b^2 + 8\pi^2(\rho - r)\rho] \cos \varepsilon - 2\pi^2 z_r \rho (3 + \cos 2\varepsilon) \}} \right) \\ &\quad \times \left(\frac{\sqrt{z_r [z_r + 2(r - \rho) \sec \varepsilon]}}{z_r} \right) \\ &= K(\rho, b, \varepsilon) \mu_m(\rho) \end{aligned} \quad (20)$$

The second term in Equation (20) represents the measured friction $\mu_m(\rho)$. Consequently, the first term indicates the introduced measurement error. This term should be equal to 1, which is now a property applying only on the case given by $b=0$ and $\varepsilon=0$. Nevertheless, in the extreme case represented by $b=51$ (mm) and a test on a mandrel designed with $\varepsilon=0$, the maximum difference between μ_r and μ_m becomes less than $7e-3$.

In an attempt to further reduce the measurement error, we assume now that a realistic range of expected friction values is given by $[\mu_{\min}, \mu_{\max}] = [0.05, 0.5]$ [13]. The corresponding ρ values are $[r_{\max}, r_{\min}] = [132.206, 103.125]$ (mm) (calculated with the aid of Equation (17)). The measurement error is one-sided: the real friction is always slightly bigger than the measured one (although this difference should be considered negligible). For very accurate measurements, one can use a modified mandrel, based on a particular ε -value (Equation (16)). This parameter ε_t depends on the fiber bundle width b , and is given by the solution of:

$$|K(r_{\min}, b, \varepsilon_t)| = |K(r_{\max}, b, \varepsilon_t)| \quad (21)$$

The parameter $\varepsilon_t(b)$ is practically linearly proportional to b ; this is illustrated in Figure 4.

In Figure 5, we provide an illustration of the error reduction achieved for a fiber bundle having a width equal to 51 (mm).

Due to the significantly small error magnitude, the corresponding mandrel shapes show hardly any differences, see Figure 6.

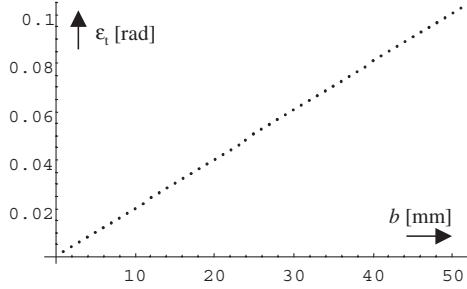


Figure 4. The modified mandrel shape parameter $\epsilon_t(b)$ as a function of the fiber bundle width.

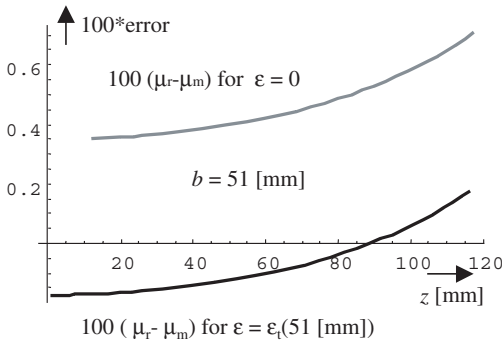


Figure 5. Measurement error for the uncorrected mandrel shape (grey line) and the corrected one (black line).

Summarizing, the solution of the simplified ODE (Equation (20)) provides a sufficiently accurate mandrel shape; the error remains always below $7e-3$ for $b \in (\text{mm})$. Only in the case of requiring an absolute measurement error below 0.002, the mandrel shape should be designed according to Equation (16), where ϵ is given by the solution of (21) for a particular roving width b .

MACHINE CONTROL

This section is associated with the determination of the required machine movements for the realization of the friction experiments. After the description of the couplings between spindle rotation, carriage translation, and feed eye inclination, we provide two equations ((22) and (24)) for relating the spindle rotation to the translation of the feed eye carriage, and maintaining the fiber speed at a constant level. The time the roving needs

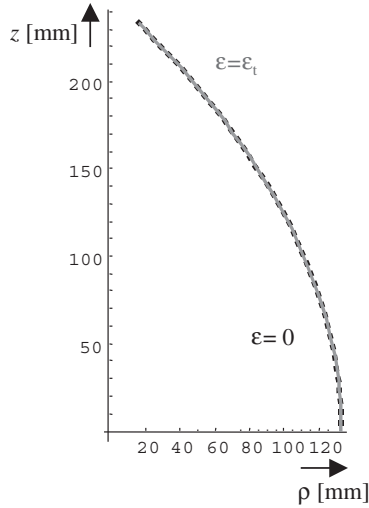


Figure 6. Mandrel shapes corresponding with $\varepsilon=0$ (black dashed line) and $\varepsilon=\varepsilon_t$ (grey continuous line) for $b=51$ (mm).

to slip off can also serve as an alternative measuring parameter for the determination of the coefficient of friction.

Movement Couplings

Due to the special mandrel shape, the measured friction is practically linear to the z -coordinate. With the assumed constant winding angle, the carriage Z is directly coupled to the corresponding z -coordinate on the mandrel. During the experiments, the spindle rotates with a speed C' (rad/s). The cross carriage X is set on a fixed value, sufficiently large to avoid collision between the mandrel and the feed eye. With the fiber bundle width denoted by b , the carriage Z becomes:

$$Z = \left(\frac{b}{2\pi} \right) C \quad (22)$$

The feed eye inclination A must ensure a tangential placement of the tow on the rotating mandrel:

$$A = \text{ArcTan} \left(\frac{d\rho}{dz} \right) = \text{ArcTan} \left(\frac{1}{z'(\rho)} \right) \quad (23)$$

The horizontal feed eye inclination is given by $A=0$ (rad). According to Equation (15) with $\varepsilon=0$ and Equations (22) and (23), we simply obtain:

$$A = \text{ArcTan}[c_1 z(\rho)] = \text{ArcTan}\left(\frac{z(\rho)}{z_r}\right) = \text{ArcTan}\left(\frac{Z}{z_r}\right) = \text{ArcTan}\left(\frac{bC}{2\pi z_r}\right) \quad (24)$$

The required machine movements are very simple and can easily be programmed in a spreadsheet. The resulting data can then be imported as a text file into the CNC controller [19]. A great advantage provided by the mandrel shape is that the machine movements can easily be determined without the aid of expensive filament winding simulation programs.

Fiber Speed

Application of a constant rotational speed of the spindle will result in a slight decrease of the consumed fiber speed S' (mm/s), when proceeding from the maximum radius ($\mu=0$) to the radius corresponding with the measured coefficient of friction value μ_m (see Figure 4). This maximum value is usually below $\mu=0.5$. At this point, the relative consumed fiber speed reduction is equal to -21.5% . The question arising now is how to vary the spindle rotation speed as a function of the feed eye position (note that C' and Z' remain coupled to each other according to Equation (22)) to ensure constant fiber speed. From Equation (17) we obtain:

$$\rho(\mu) = \frac{z_r}{2} \cos \varepsilon (1 - \mu^2) + r \quad (25)$$

Due to the linearity between μ and z , (or Z), the parameter μ can be treated as the dimensionless carriage coordinate ζ ($=Z/z_r$) proceeding from 0 to 1. The aimed constant consumed fiber speed is denoted by $S'(t)$. With the relation $S'(t) = \rho(\mu)C'(t)$, the required $C'(\zeta)$ profile in rpm is given by (note that r and z_r are given in (mm)):

$$C'(\zeta) = \frac{30 S'(t)}{\pi \rho(\zeta)} \text{ (rpm)} \quad (26)$$

An alternative formulation is to use discrete ζ -values given by $i\Delta Z/z_r$. The $C'(\zeta)$ profile for $r=15$ (mm) and $z_r=235$ (mm) and $S'(t)=500$ (mm/s) is given in Figure 7.

The set of CNC control data is based on a constant ΔZ increment. The corresponding ΔC increment is given by Equation (22). With the dimensionless cumulative value for Z ($=i\Delta Z/z_r$) and Equation (30),

the required rotational speed C' for every increment can be determined. The corresponding feed eye inclination is given by Equation (24).

An alternative fiber speed control strategy can be obtained through the proper determination of the corresponding time increments as a function of ζ (some controllers may require such an input format). With a constant fiber speed S' , and a roving width b , the time increment to complete the i th circuit is given by:

$$\Delta t(i) = \frac{2\pi\rho(i(b/z_r))}{S'} \quad (27)$$

The required time for reaching the n th circuit corresponding with the measured coefficient of friction, is:

$$t(b, \mu_m) \approx \sum_{i=0}^n \frac{2\pi\rho(i(b/z_r))}{S'} \quad \text{with } n = \text{Integerpart of } \frac{\mu_m z_r}{b} \quad (28)$$

We assume the maximum expectable coefficient of friction as equal to 0.5. The dimensionless carriage ζ will run from 0 to 0.5. For a simple approximation (for example to be used in spreadsheets) of the time as a function of ζ , one may proceed to the elaboration of Equation (28). The discrete character of Equation (28) provides a nonzero time value for the initial parameter $i=0$, so a correction has to be added. The result is:

$$t_{\text{appr}}(b, \zeta) = -\frac{\pi(b + z_r\zeta)[b\zeta + 2z_r(\zeta^2 - 3) - 12r]}{6bS'} - \frac{\pi(2r + z_r)}{S'}(1 - \zeta^{a(b)})$$

where $\begin{cases} b < 10 \text{ (mm)}: a = 1 \\ b > 10 \text{ (mm)}: a = b/10c \end{cases}$ (29)

The exact value for the time required to reach ζ is given by [5]:

$$t_{\text{exact}}(b, \zeta) = \frac{1}{S'} \int_{l=\rho(\zeta)}^{l=r_{\text{max}}} \frac{\sqrt{1 + z^2(l)}}{\cos \alpha(b, l)} dl \quad (30)$$

where $\alpha(b, l)$ is given by Equation (18). The implementation of this integral however, involves rather complicated functions. In Figure 8, we provide the relative error generated by Equation (29) when compared to the exact solution (30).

For the most typical filament winding applications range corresponding to $b = [5, 30]$ (mm) and $\mu = [0.1, 0.5]$, the error remains below 3%.

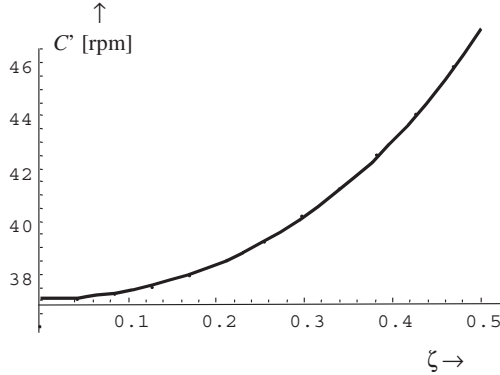


Figure 7. Spindle speed profile as a function of the dimensionless carriage.

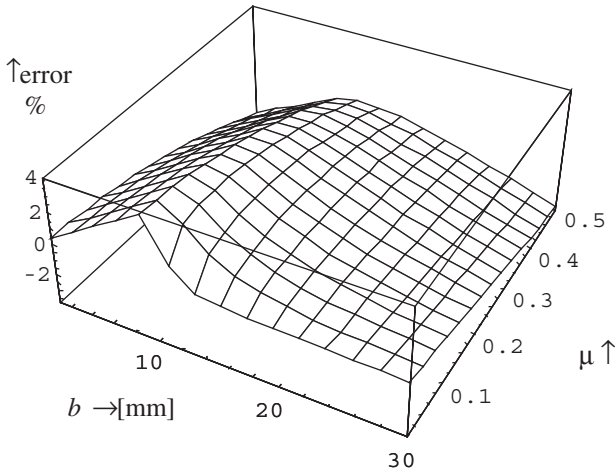


Figure 8. Relative error of the approximated experiment time vs the exact one for the expected range of coefficient of friction values.

For a certain ζ (or Z/z_r) value, with the restriction of a practically constant fiber speed (within a deviation of $\pm 3\%$), the required time increments can be obtained by Equation (29). As indicated in the previous section, the time interval from the beginning of the experiment until slippage can be translated into the corresponding ζ -coordinate (which can directly be interpreted as the measured coefficient of friction). For this translation however, we should take into account that application of Equation (29) may introduce an error of (maximally) 3%. Consequently, it is preferable to use Equation (30) for that purpose.

EXPERIMENTS

Setup

For the acquisition of the coefficients of friction related to various winding process parameter combinations, we use here the specially designed mandrel as outlined in “Nongeodesic Fiber Trajectories on Generic Shells of Revolutions” and depicted in Figures 2 and 3. Due to the implemented meridian profile, the coefficient of friction is linearly proportional to the carriage position Z . The left side of the mandrel is characterized by $[\rho, Z] = [132.5, 0]$ (mm) and $\mu = 0$. The curved mandrel part ends at $[\rho, Z] = [15, 235]$ (mm) and $\mu = 1$. The aluminum mandrel surface is polished. The mandrel is attached on a CNC-controlled lathe-configured filament-winding machine (Figure 9).

To determine the point where slipping starts, we used a video camera with high shutter speed (600), see Figures 9 and 10. The mandrel is utilized with a fixed benchmark indicating the carriage position Z (marking: 5 (mm)). In addition, a second benchmark on the mandrel indicates its rotational position with a marking of 20° (Figure 10). A carriage stroke equal to the roving width b corresponds with a spindle rotation of 360° .

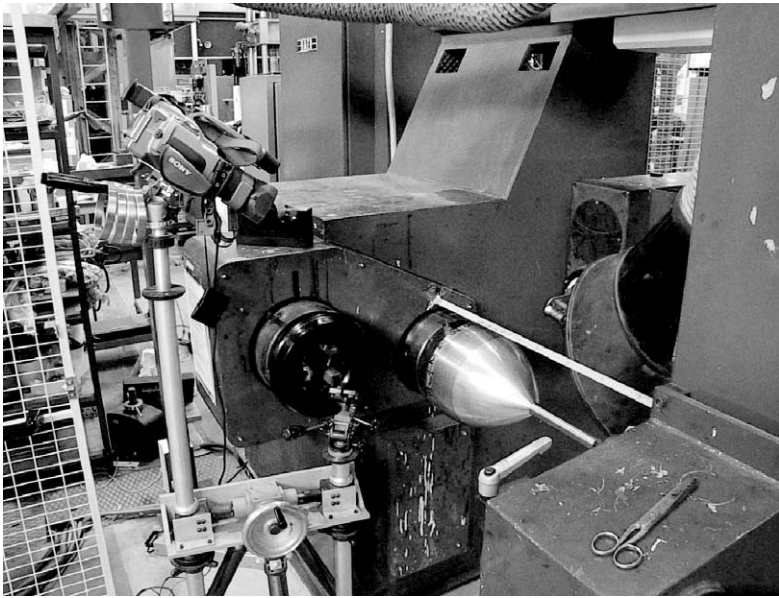


Figure 9. The complete test setup, including video camera and suction unit.



Figure 10. The mandrel with benchmarks for the carriage Z and the rotation C.

A 20° -propagation on the angular benchmark corresponds with a carriage stroke equal to $b/18$.

At a certain point, the tow will start slipping on the mandrel; this point provides the initial value for the coefficient of friction to be measured. This phenomenon is followed by a complete separation of the tow from the mandrel surface. This separation is referred to as ‘catastrophic slipping’ [13].

Measurement Error Estimation

The high shutter speed camera provides sufficient accuracy for the determination of the slippage point. However, the judgment of whether slipping occurs is rather subjective. We assume here that the observer of the experiment is able to provide this judgment within an accuracy of 50% on the angular benchmark, placed on the mandrel. This uncertainty corresponds with 10° on the benchmark, thus $1/36$ of the roving width. An additional error is introduced by the shape of the mandrel; as explained in “Determination of Coefficient of Friction,” the linearity error is maximally 0.7%. The maximum expected value for the measured coefficient of friction is 0.5. This value, in combination with the shape inaccuracy, leads to an absolute error of $\Delta\mu = 0.0035$. Furthermore, the mandrel is manufactured with an accuracy of ± 0.01 (mm). The influence of this tolerance on the

measurements however, can be neglected. At the beginning of the experiment, the carriage position must be referenced. For this procedure, we assume a tolerance ΔZ_0 of ± 1 (mm). The total absolute error becomes:

$$E_{\text{abs}}(b) = \left(\frac{\Delta Z_0}{z_r} + \Delta\mu \right) + \frac{b}{36z_r} \quad (31)$$

With $z_r = 235$ (mm), the result is depicted in Figure 11.

Performed Series

Several winding parameters can possibly influence the amount of available friction between placed roving and mandrel. Although some of these parameters are not expected to have substantial impact on the coefficient of friction values, we include them here to cover the complete set of possible filament winding processes. The investigated series are based on the following variables:

- Winding speed (spindle rotation: 3.6, 12, and 60 (rpm))
- Fiber tension (narrow rovings: 1–5 (N), broad rovings: 5–15 (N))
- Roving morphology: width (0.5, 1, 1.5, 2, and 3 (mm)) and twisted/untwisted yarns
- Fiber materials (glass, carbon)
- Wet/dry winding
- Surface roughness of the mandrel

The expected values for the coefficients of friction lay in the range [0.1, 0.5]. With regard to the roving speed, we apply for the experiments here a constant value for the rotational speed of the spindle C' . As outlined in “Machine Control,” when proceeding with the roving toward higher

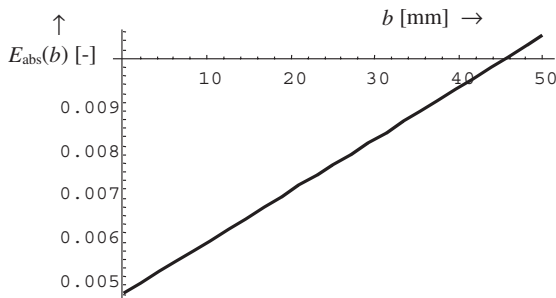


Figure 11. Estimated absolute error for the measured coefficient of friction as a function of the roving width.

Table 2. Expected friction values and their corresponding roving speeds for various C' -values.

Coefficient of friction	Carriage Z (mm)	Mandrel radius ρ (mm)	Fiber speed (m/s) at $C' = 3.6$ (rpm)	Fiber speed (m/s) at $C' = 12$ (rpm)	Fiber speed (m/s) at $C' = 60$ (rpm)
0.1	23.5	131.325	0.0495	0.165	0.825
0.2	47.0	127.800	0.0482	0.161	0.803
0.3	70.5	121.925	0.0460	0.153	0.766
0.4	94.0	113.700	0.0429	0.143	0.714
0.5	117.5	103.125	0.0389	0.130	0.648

Z-values, a roving speed reduction is expected. The roving speed values are given in Table 2.

RESULTS

For every parameter combination (winding speed, tension, etc.) we carried out three experiments. The provided results show the calculated mean values. The results are presented per examined parameter. In order to isolate a parameter, for example speed, we calculated the average friction value of the complete set of experiments for a certain winding speed. The influence of for example the winding speed on the resulting friction however, may strongly be affected by the fiber tension or mandrel surface quality. Consequently, the results per examined parameter provide only a general idea about the effect that an input parameter can have on the final result.

Winding Speed

The tests corresponding to the ‘winding speed’ series have been carried out with $C' = \{3.6, 12, 60\}$ (rpm) (when an absolutely constant fiber speed is desired, the rotational speed of the spindle must be varied according to the corresponding radii (“Machine Control”)). The obtained friction values corresponding to catastrophic slipping are practically the same as the values for initial slippage of the fibers. The mean standard deviations are in the order of $[0.01, 0.02]$. The averaged result of the experiments clearly indicates that the influence of the winding speed on the measured friction is generally negligible and remains in the order of $[0, 0.02]$; this observation is valid for dry as well as wet winding. In conclusion, the influence of the winding speed on the friction between tow and mandrel is negligible.

Roving Tension

Depending on the dimensions of the examined fiber bundles, the tension has been limited in several cases to avoid tow failure. As observed by the winding speed series, catastrophic slipping occurs at practically the same place as the initial slippage. The differences between the obtained experimental data are negligible (in the order of 0.015). The standard deviation is in the order of [0.014, 0.018]. From these series, we can conclude that the fiber tension does not significantly affect the obtained friction values.

Fiber Materials

To ensure the usability of the generated results, we selected some typical carbon and glass fibers. The carbon rovings are summarized in Table 3.

The examined glass fiber bundles are given in Table 4.

To isolate the influence of the fiber material on the coefficient of friction, the experimental series have been limited to dry fiber bundles. The results indicate that the difference between carbon fibers and glass fibers is negligible (in the order of 0.003). The standard deviation remains in the order of [0.008, 0.01] and the obtained values belong to the [0.178–0.181]-range.

Table 3. The examined carbon fiber bundles.

Manufacturer	Torayca (Japan)	Soficar Torayca (France)	Soficar Torayca (France)
Type	T300	T300	T300
Twisted/untwisted	Twisted	Untwisted	Untwisted
Number of filaments	1000	3000	6000
Lot-nr	080045	F113013	F110083
Approximate fiber width	0.5 (mm)	1.5 (mm)	2.5 (mm)

Table 4. The examined glass fiber bundles.

Manufacturer	PPG fiber glass	PPG fiber glass	PPG fiber glass	Vetrotex	Scott Bader
Type/Lot	ECDE 75 1/0 0.7Z 610	ECDE 150 1/0 1.0Z 631	611 EC 11 136 Z20	EC-13-136 TD22 V379	320 Tex. Roving
Twisted/ untwisted	Twisted	Twisted	Twisted	Untwisted	Untwisted
Approximate fiber width	0.3 (mm)	0.5 (mm)	1 (mm)	1–1.5 (mm)	2–3 (mm)

However, Di Vita et al. [3] obtained $0.1 \leq \mu_{\text{carbon}} \leq 0.125$ and $0.275 \leq \mu_{\text{glass}} \leq 0.3$, which is a significant difference. Since the cited experimental study is comparable with the method presented here, the difference is probably caused by the surface treatment of the fibers used here or the surface quality of the involved bullet.

Roving Morphology

The fiber bundle width and the characterization twisted/untwisted are closely related to each other. In the tests performed here, the rovings having a width from 0.3 to 1 (mm) are twisted, while the broader ones are untwisted. The results for slipping start are presented in Figure 12. The depicted results do not include the case of wet winding, since this is expected to flatten out the influence of the roving width on the measured coefficient of friction.

The depicted results indicate that an increased roving width tends to raise the coefficient of friction. A possible explanation for this phenomenon is outlined in “Determination of Coefficient of Friction,” formulated in Equation (20), and indirectly depicted in Figure 5. Nevertheless, the results generated by Equation (20) are too small for explaining the measured differences. Consequently, the tendency toward higher friction values can probably be explained by an increased interaction between the yarns. Since every yarn is subjected to a different normal curvature across the fiber width, interference between them is very likely to occur; the broader the tape, the bigger the total velocity difference between the inner and outer yarns. This scenario however, has not been verified. Furthermore, the mean standard deviation for the presented values remains in the range [0.01, 0.02].

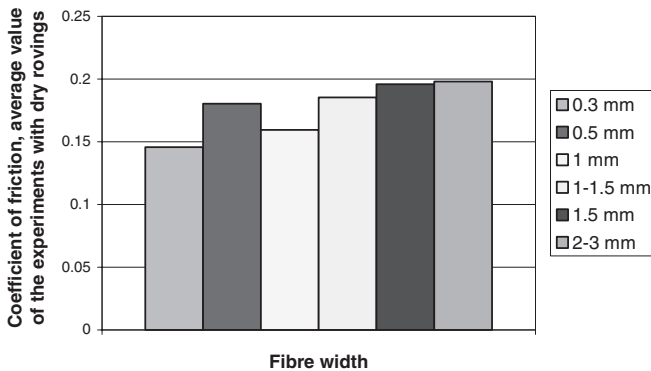


Figure 12. Averaged influence of the roving width on the measured coefficients of friction at slipping start.

Wet versus Dry Winding

For the performance of the wet winding experiments, the mandrel has been covered with epoxy resin of the type VE 2908 KA/VE 4908 KB, manufactured by Bakelite AG. The potlife is 5–6 h. It is believed that this mandrel coverage can result in an acceptable simulation of winding with impregnated fibers. As a result of the tests performed here, the obtained coefficients of friction did not show any time dependency. Consequently, it is believed that the resin viscosity has no considerable impact on the coefficient of friction, at least in this particular case. The results are depicted in Figure 13.

The tests have been performed on the polished surface of the aluminum mandrel. The comparison between dry and wet winding reflects on identical ‘winding speed/tension/roving dimensions/fiber materials’ sets. In general, we can conclude that the coefficients of friction for wet fibers are approximately three times as high as for dry fibers. The values for catastrophic slipping are even slightly higher. Nevertheless, the observed differences are rather small. The standard deviation for the presented results is within the order of 0.006 for dry winding and 0.03 for wet winding.

The results obtained here do not completely agree with [9] who reported $0.24 \leq \mu_{\text{dry}} \leq 0.39$ and $0.29 \leq \mu_{\text{wet}} \leq 0.37$. In addition, Lossie and van Brussel [8] report $0.2 \leq \mu_{\text{wet}} \leq 0.34$ while Scholliers and van Brussel [14] report and $0.2 \leq \mu_{\text{wet}} \leq 0.4$. Furthermore, Park et al. [12] (who refers to [14]) report $\mu_{\text{wet}} = 0.2$ and $\mu_{\text{dry}} = 0.39$. In conclusion, the determination of whether dry or wet winding will provide elevated values for the coefficient of friction is probably dependent on more parameters like the quality,

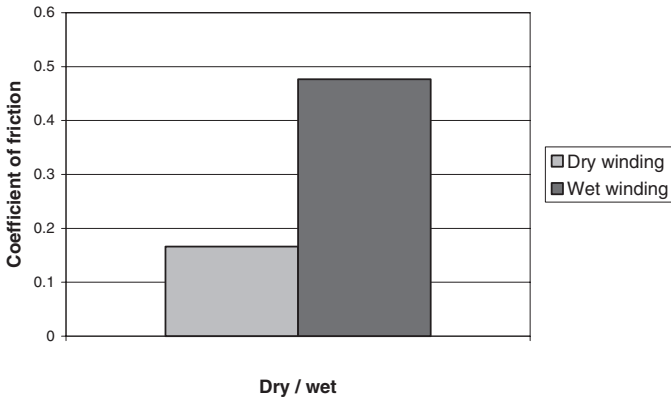


Figure 13. Dry winding vs wet winding (averaged results).

potlife and manufacturer of the resin, mandrel surface quality, fiber materials, etc. Perhaps standardization would provide more reliable data.

Mandrel Surface

The surface quality of the mandrel is obviously a parameter having a great impact on the measured coefficients of friction. In the experiments performed here, we examined three characteristic surfaces: polished aluminum, mandrel smoothly covered with a dry epoxy layer (Araldite LY 5052/HY 5052), and roughened epoxy layer (achieved by a sandpaper with grain size 120). The obtained results are depicted in Figure 14.

As expected, the epoxy layers provide considerably higher friction values. A remarkable aspect presented in the figure is that the averaged difference between the smooth and roughened epoxy surface data is very small. As observed from the comparison between wet and dry winding, the friction becomes for both epoxy layers approximately three times higher. The related standard deviations remain in the order of [0.008, 0.03].

A more reliable way to depict the data should involve the presentation of the measured coefficients of friction as a function of the average surface roughness (R_a). This representation format however, does not still provide reliable conclusions. An important parameter influencing the sensitivity of the friction for the surface roughness is the roving morphology. In Figure 15, we provide the average friction values for the untwisted carbon fiber roving T300 with 3000 filaments and a total width of 1.5 (mm).

As expected, the measured friction increases with the mandrel surface roughness. For a twisted fiber bundle however, this statement might not be

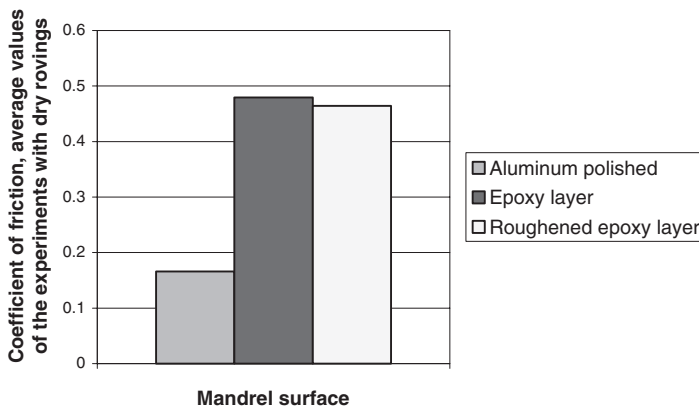


Figure 14. Measured coefficients of friction for various mandrel surface qualities (roughness).

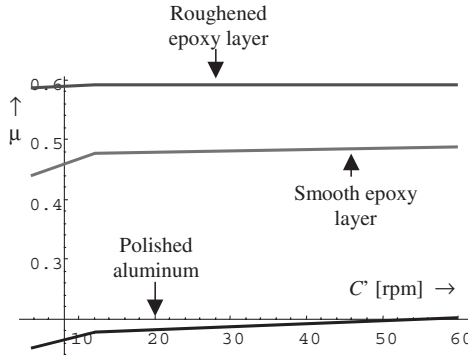


Figure 15. Measured friction for various mandrel surface qualities (dry untwisted carbon roving with $b = 1.5$ (mm)).

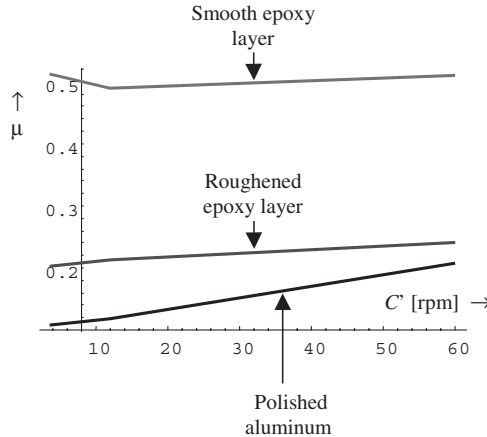


Figure 16. Measured friction for various mandrel surface qualities (dry twisted glass roving with $b = 0.3$ (mm)).

realistic. In Figure 16, we present the surface roughness response of a twisted glass fiber bundle (ECDE 75, $b = 0.3$ (mm)).

The value for the coefficient of friction corresponding to the smooth epoxy layer is considerably larger than the original one (polished aluminum). On the roughened epoxy layer however, the friction drops significantly. This can possibly be explained by rolling of the roving over the surface instead of slipping. Nevertheless, this statement has to be further examined. The combination of friction values related to both sliding and rolling results in the small differences (smooth epoxy vs. roughened epoxy) presented in Figure 16.

CONCLUSIONS

In this paper, we presented an extensive treatment of friction experiments for filament winding applications. The main objective of this paper is the description of the method and presentation of the results related to experiments for the determination of the coefficient of friction between the mandrel and the applied roving for filament winding applications. The involved mandrel surface is specially designed for providing a linear relation between the measured coefficient of friction and the feed eye carriage translation of the winding machine. The roving slippage locus has been determined with the aid of a high shutter speed camera. The performed experiments correspond to various filament winding process related parameters like fiber speed, roving tension, fiber dimensions and materials, wet versus dry winding, and surface quality of the mandrel.

The advantages provided by the implementation of the proposed mandrel geometry on a filament-winding machine are:

- Realistic simulation of the fiber behavior during filament winding processes
- Facilitated determination of the coefficient of friction (optical or by means of a chronometer)
- Improved stability and accuracy for the measurements (due to the linearly proportional relation between coefficient of friction and carriage)
- Simple machine control (suitable for spreadsheet programming)

The most important property of the proposed method is that the linearity (carriage vs. expected coefficient of friction) ensured by the mandrel shape, makes a low-cost experimental friction determination procedure feasible, without the need of advanced filament winding simulation programs. The complete set of errors generated by simplifications in the mandrel geometry and machine control remains considerably small. The costs for performing the friction experiments are rather low; this is mainly caused by the general applicability and reusability of the mandrel.

The measurements clearly indicate that the most important parameters influencing the coefficient of friction are the surface quality, fiber bundle morphology (twisted/untwisted), and the eventual fiber impregnation. The influence of the winding speed, roving tension, and fiber bundle material can be considered as negligible. The effect of surface quality on the resulting friction is significant; the coefficient of friction tends to increase with increasing surface roughness. For rather rough surfaces however, the resulting coefficient of friction depends strongly on the fiber bundle morphology: broad untwisted rovings tend to slide, while the twisted bundles prefer to roll over the surface. An unexpected observation is that

the coefficient of friction for impregnated fibers is clearly higher than for dry fibers. These observations do not completely agree with previously reported results [3,8,12,14]. Nevertheless, it is believed that these discrepancies are probably caused by differences in the surface quality of the mandrel, the surface treatment of the involved fibers and/or the resin quality and potlife. This statement however, is rather subjective.

The results obtained here represent only general tendencies; for a more reliable determination of the available coefficient of friction, one should perform experiments with the specific winding parameter combinations that are expected to be applied at the production stage. For the design of nongeodesically wound objects however, we can provide the following rules (for a conservative estimation, one could extract 0.05 from the presented values):

- Dry fiber bundles (both twisted and untwisted) on a polished aluminum surface: $\mu = 0.15$
- Twisted dry fiber bundles (small b) on a roughened dry epoxy surface: $\mu = 0.20$
- Impregnated (wet) fiber bundles on a polished aluminum surface: $\mu = 0.4$
- Dry fiber bundles on smooth dry epoxy surface: $\mu = 0.5$
- Untwisted dry fiber bundles (moderate b) on a roughened epoxy surface: $\mu = 0.6$

The standard deviation for every measured series is smaller than the estimated error; this property indicates that the measurements can generally be considered as reliable, without the presence of a systematic error.

It is strongly advisable to separately obtain friction data for thermoplastic composites, since their physiology is rather different. At the same time, contrary to thermoset materials, the measured coefficient of friction might be strongly dependent on the viscosity of the matrix. Furthermore, we strongly recommend further experimental investigations, preferably with addition methods to clarify the coefficient differences reported by several authors.

NOMENCLATURE

Latin

- A = feed eye inclination angle (rad)
- a = shape function, exponent (length, -)
- b = shape function, roving width (length)
- C = spindle rotation (rad)

- c = constant (length⁻¹)
 E = coefficient of the first fundamental form (length²)
 E_f = absolute measurement error
 f = contact force per unit length (N/length)
 F = coefficient of the first fundamental form (length²)
 G = coefficient of the first fundamental form (length²)
 K = shape error function (-)
 k = curvature (length⁻¹)
 n = circuit number (-)
 R = curvature radius (length)
 r = minimum mandrel radius (length)
 S = vector function describing a surface
 t = time (s)
 X = cross carriage (length)
 x = body related coordinate (length)
 y = body related coordinate (length)
 Z = carriage (length)
 z = body related coordinate, meridian profile function (length)

Greek

- α = winding angle (rad)
 ε = angular deviation (rad)
 ζ = dimensionless carriage
 μ = coefficient of friction (-)
 ρ = radius (length)
 ϕ = parallel angle (rad)
 ΔZ_0 = carriage referencing error (length)
 $\Delta\varphi$ = normal angular increment (rad)
 $\Delta\omega$ = lateral angular increment (rad)

Indices

- 0 = distinction for constants
 1 = distinction for constants
 g = geodesic
 m = meridional, measured
 \max = maximum
 \min = minimum
 n = normal
 p = parallel
 r = maximum z -value, real

s = simplified
 t = tuned
 μ = lateral

Special Functions and Operators

\sec = $1/\cos$
 ArcTan = arc tangent (rad)
 Integerpart = the integer number contained in a real quantity
 Δ = increment
 $\|$ = absolute value
 $'$ = first derivative
 $''$ = second derivative

ACKNOWLEDGEMENTS

The authors wish to gratefully thank Mr. Martin Renggli for his contributions to both the design and experimental work related to the friction measurements. They are also thankful to all the laboratory people who contributed with their expertise.

REFERENCES

1. Beukers, A. and Hinte, E. van (1998). *Lightness: The Inevitable Renaissance of Minimum Energy Structures*, 010 Publishers, Amsterdam.
2. Rosato, D.V. and Grove, C.S. (1964). Filament Winding: Its Development, Manufacture, Applications, and Design, In: *Polymer engineering and technology*, Interscience, New York.
3. Di Vita, G., Grimaldi, M., Marchetti, M. and Moroni, P. (1990). The Filament Winding Manufacturing Technique: Studies on the Determination of the Friction Coefficient and on the Optimisation of Feed-eye Motion, In: *Proceedings of the 22nd International SAMPE Technical Conference*, pp. 972–979.
4. Koussios, S., Bergsma, O.K. and Mitchell, G. (June 2002). Non-geodesic Filament Winding on Generic Shells of Revolution, In: *Proceedings of ICCM 10*, Brugge.
5. Koussios, S. and Bergsma, O.K. (2002). Uninterrupted Hoop- and Polar Fibre Paths on Cylindrical Pressure Vessels Using Non-geodesic Trajectories, In: *Proceedings of the 17th Annual Conference of the American Society for Composites*, West Lafayette, IN.
6. Carvalho, J.D., Lossie, M., Vandepitte, D. and Van Brussel, H. (1995). Optimization of Filament-wound Parts Based on Non-geodesic Winding, *Composites Manufacturing*, 79–84.
7. Liang, Y.D., Zou, Z.Q. and Zhang, Z.F. (1996). Quasi-geodesics- A New Class of Simple and Non-slip Trajectories on Revolutionary Surfaces, In: *Proceedings of the 28th International SAMPE Technical Conference*, pp. 1071–1079.
8. Lossie, M. and Brussel, H. van (1994). Design Principles in Filament Winding, *Composites Manufacturing*, 5(1): 5–13.
9. Li, Xian-li and Lin, Dao-hai (1987). Non-geodesic Winding Equations on a General Surface of Revolution, In: *Proceedings of the 7th ICCM/ECCM Conference*.

10. Wells, G.M. and McAnulty, K.F. (1987). Computer Aided Filament Winding Using Non-geodesic Trajectories, In: *Proceedings of the Second ICCM/ECCM Conference on Composite Materials*, London.
11. Mitchell, G. (July 2001). Non-geodesic Filament Winding Equation and Solution for Surfaces of Revolution, Internship Report, Structures and Materials Laboratory, Faculty of Aerospace Engineering, Delft University of Technology, Delft.
12. Park, Jae-Sung, Hong, Chang-Sun, Kim, Chun-Gon and Kim, Cheol-Ung (2002). Analysis of Filament Wound Structures Considering the Change of Winding Angles through the Thickness Direction, *Composite Structures*, **55**: 63–71.
13. Renggli, M. (June 2003). Friction Tests for Filament Winding, Internship Report, Structures and Materials Laboratory, Faculty of Aerospace Engineering, Delft University of Technology, Delft.
14. Scholliers, J. and Brussel, H. van (1994). Computer-integrated Filament Winding: Computer-integrated Design, Robotic Filament Winding and Robotic Filament Winding and Robotic Quality Control, *Composites Manufacturing*, **5**(1): 1103–1112.
15. Simoes, J.A.O., Wu, S.T. and Loseries, F. (1993). Visual Simulation of the Geodesic and Non-geodesic Trajectories of the Filament Winding, *Graphics Modelling and Visualization in Science and Technology*, 199–215.
16. Gray, A. (1993). *Modern Differential Geometry of Curves and Surfaces*, CRC Press.
17. Kreyszig, E. (1999). *Advanced Engineering Mathematics*, John Wiley & Sons, Inc., New York.
18. www.mathworld.wolfram.com
19. *Baer Filament Winding Machine Instruction Manual*, Josef Baer Maschinenfabrik D-7987 Weingarten/Württ.